SIMULATING GUITAR DISTORTION CIRCUITS USING WAVE DIGITAL AND NONLINEAR STATE-SPACE FORMULATIONS

David T. Yeh and Julius O. Smith

Center for Computer Research in Music and Acoustics (CCRMA)
Stanford University, Stanford, CA
[dtyeh|jos]@ccrma.stanford.edu

ABSTRACT

This work extends previous research on numerical solution of nonlinear systems in musical acoustics to the realm of nonlinear musical circuits. Wave digital principles and nonlinear state-space simulators provide two alternative approaches explored in this work. These methods are used to simulate voltage amplification stages typically used in guitar distortion or amplifier circuits. Block level analysis of the entire circuit suggests a strategy based upon the nonlinear filter composition technique for connecting amplifier stages while accounting for the way these stages interact. Formulations are given for the bright switch, the diode clipper, a transistor amplifier, and a triode amplifier.

1. INTRODUCTION

This research attempts to model and simulate highly nonlinear circuits used primarily for electric guitar effects. Such efforts aim to preserve the heritage of circuits whose components, such as vacuum tubes, or particular vintage transistors, are becoming increasingly rare. Circuit schematics and accurate device model equations can sufficiently model circuit behavior. Using these with Kirchhoff's Current Law (KCL) and Kirchhoff's Voltage Law (KVL), one can derive a system of nonlinear equations that accurately replicates a circuit's input-to-output relationship over time. By exploiting the progress of contemporary digital computing power, modeling vintage circuits based on archives of their circuit schematics and device characteristics can ensure that the unique sound of these circuits will be available for future generations of musicians.

Numerical simulation of lumped nonlinear systems has been studied extensively in the literature [1–7]. The musical acoustics or digital audio effects community has developed two prevailing methods for simulating ordinary differential equations with nonlinearities based on wave digital principles or directly solving a nonlinear state-space system. Both methods have been applied to the same types of problems in nonlinear musical acoustics and are also applicable to certain classes of nonlinear circuits used for musical effects.

This work extends attempts to simulate musical circuits based upon solving ordinary differential equations [7–10]. The motivation for this work is to investigate block-based modeling techniques [11] applied to a more complete simulation of electronic circuits used in musical effects processing. Circuits naturally divide into stages [12] which may interact with adjacent stages, or "load" them, and are apt for description as a two-way signal flow diagram as in [11]. This work presents examples of how circuits may be represented as blocks in such a modeling scheme. Various schemes exist that account for the mutual interaction between blocks [4, 11, 13].

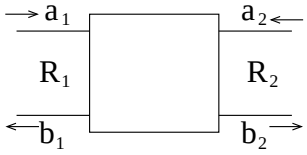

Figure 1: Two-port scattering element defines network blocks using incident wave a, reflected wave b, and port impedance R.

This paper reviews the wave digital formulation for representing circuits as digital filters, and the K-method of computational musical acoustics, and then demonstrates the applicability of these techniques to circuits in guitar electronics: the bright switch, the diode clipper, a transistor amplifier, and a triode amplifier.

2. REVIEW OF METHODS IN COMPUTATIONAL MUSICAL ACOUSTICS

2.1. Wave Digital Formulation

The wave digital formulation [14] views the linear N-port circuit network as a scattering junction, replacing voltage V and current I variables that define a single port by incident A and reflected B waves, and a port impedance $R \geq 0$, as depicted in Fig. 1 for a two-port. Doing so allows instantaneous reflections to be eliminated by matching port impedances when ports of different blocks are connected together, resulting in a computationally realizable wave digital filter (WDF) structure.

The variable transformation to the wave domain is

$$\begin{aligned} A &= V + RI \\ B &= V - RI \end{aligned} \tag{1}$$

and the inverse formulation exists $\forall\, R \geq 0$.

2.1.1. Wave digital elements

In the wave digital filter, circuit elements such as resistors, capacitors and inductors become port impedances and delay, if applicable, as shown in Tab. 1. They are computed by substituting (1) into the Kirchhoff definitions of the elements and computing the reflected waves due to the change in impedance from the port to the element. Usually the port impedance is chosen such that the instantaneous reflection is matched, resulting in a reflection-free port (RFP).

Element	Port impedance	Reflected wave
Resistor R	$R_p = R$	$b[n] = 0$
Capacitor C	$R_p = T\,/\,2C$	$b[n] = a[n-1]$
Inductor L	$R_p = 2L\,/\,T$	$b[n] = -a[n-1]$
Short circuit	$R_p = X$	$b[n] = -a[n]$
Open circuit	$R_p = X$	$b[n] = a[n]$
Voltage source V_s	$R_p = X$	$b[n] = -a[n] + 2V_s$
Current source I_s	$R_p = X$	$b[n] = a[n] + 2R_pI_s$
Terminated V_s	$R_p = R_s$	$b[n] = V_s$
Terminated I_s	$R_p = R_s$	$b[n] = R_pI_s$

Terminated V_s Terminated I_s

Table 1: Wave digital elements: Port impedances and reflected waves. The last two elements are sources lumped with a resistance as shown. Elements with unmatched port impedances can be set to any non-negative port impedance $R_p = X$.

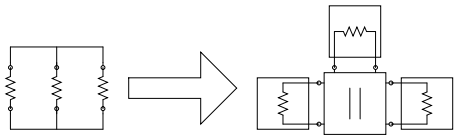

(a) Parallel

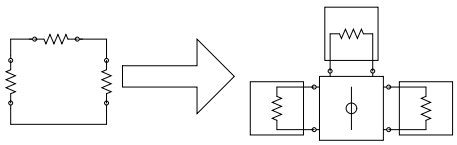

(b) Series

Figure 2: Three-port adaptors and corresponding circuit schematic

2.1.2. Interconnections of elements: wave digital adaptors

The topology of the circuit is represented by adaptors, which compute the scattering among connected ports given their port impedances. Because connections can often be described in terms of series and parallel electrical arrangements, series and parallel adaptors have been studied in detail and are used for connecting elements in wave digital filters. Parallel and series adaptors in the three-port case are shown schematically in Fig. 2. The scattering relations for elements and adaptors are derived by substituting (1) into the Kirchhoff equations defining the element or adaptor.

The scattering relations for N-port parallel adaptors are given by

$$\gamma_\nu = \frac{2G_\nu}{G_1 + G_2 + \cdots + G_n}$$

$$a_p = \gamma_1 a_1 + \gamma_2 a_2 + \cdots + \gamma_n a_n$$
$$b_\nu = a_p - a_\nu,$$

where γ_ν is the scattering parameter for port ν, $\nu = 1 : \mathrm{N}$, a_p is a parallel junction wave variable, and b_ν is the reflected wave for port ν.

The scattering relations for N-port series adaptors are given by

$$\gamma_\nu = \frac{2R_\nu}{R_1 + R_2 + \cdots + R_n}$$

$$a_s = a_1 + a_2 + \cdots + a_n$$
$$b_\nu = a_\nu - \gamma_\nu a_s$$

where a_p is a series junction wave variable, and b_ν is the reflected wave seen at port ν.

The reader is referred to the comprehensive tutorial by Fettweis [14] for the scattering relations of other elements and adaptors.

Each adaptor can have at most one reflection free port (RFP), identified by a symbol T on the input terminal, whose impedance is matched to the equivalent impedance of all the other ports combined. Because of this, adaptors naturally form a directed tree structure (see Figs. 4, 7 below) with the RFP oriented towards the root of the tree.

The entire tree in the classical WDF formulation naturally admits only one element with an instantaneous reflection, which must be placed at the root of the tree. All other elements must not have an instantaneous reflection. While the tree arrangement is suggested in [14], a more thorough development is presented in [2].

2.1.3. Nonlinear wave digital elements

Nonlinear elements are also derived by substitution of (1) into the Kirchhoff definition of the element, and solving for the reflected wave b [15]. This often produces an instantaneous reflection, which in the classical WDF, must be placed at the root of the tree. Thus, WDFs can handle only a single nonlinearity, although modified approaches might be able to handle more [16].

Wave digital filters can also implement nonlinear reactances such as capacitors and inductors by defining an auxiliary port to the element whose wave variables correspond to the state variables of the reactance. For example, for a nonlinear capacitor $Q = C(V)\,V$, the wave variables at the auxiliary port would be defined in terms of charge Q and voltage V. The transformed variable definitions can then be used in the defining equations of the nonlinear reactance. The reader is referred to [1, 17] for detailed derivations and usage.

2.1.4. Practical considerations

Because WDFs are often arranged in a tree structure, with data dependency flowing from the leaves up to the root, and then from the root back down to the leaves, it is convenient to label the wave signals in terms of u for signals going up the tree (through the RFP, marked with T), and d for signals traveling down the tree [2, 11]. Otherwise, naming signals in terms of incident and reflected waves between WDF components can quickly become unwieldy.

Once the WDF elements and adaptors are defined, the WDF tree is sufficient to represent its computational structure. The following examples will present their algorithms as WDF trees.

2.1.5. Computational complexity

WDFs take advantage of the linear complexity of parallel and series adaptors to produce very compact signal processing code. In

particular, N-port parallel and series adaptors with one reflection free port incur a computational cost of $N-1$ multiplies and $2N-2$ adds. In comparison, general N-port scattering matrices require a full matrix-vector multiply, and a direct implementation would have N^2 multiplies and $(N-1)^2$ adds.

A WDF with N elements synthesized as a binary tree of 3-port parallel and series adaptors as described in [11] would have $N-2$ 3-port adaptors. The computational cost of a straightforward implementation of these adaptors would be $2N-4$ multiplies and $4N-8$ adds. Thus, the linear order of complexity is preserved globally. Clearly, if a circuit can be decomposed into parallel and series connections, using adaptors instead of full scattering matrices to represent the circuit presents a great computational advantage.

2.2. State-Space with Memoryless Nonlinearity (SSMN)

Most nonlinear characteristics for devices in guitar circuits can be described as memoryless nonlinearities. The circuits can therefore be represented in state-space form with separate terms for the linear and nonlinear parts of the system. Numerical solution of such systems results in a discrete-time state-space system with an embedded memoryless nonlinearity. This class of solvers may be referred to as State-Space with Memoryless Nonlinearity (SSMN) solvers.

2.2.1. K-method

An SSMN approach was developed in computational musical acoustics as the so-called K-method [3], using a particular matrix representation of nonlinear state-space systems. Note that the variable names are modified here from the original exposition to clarify the relationship with standard state-space formulations, and to aid interpretation for the following examples.

The K-method deals with a broad class of systems that can be expressed in the form

$$\dot{\mathbf{x}} = \mathbf{A}\mathbf{x} + \mathbf{B}\mathbf{u} + \mathbf{C}\mathbf{i}, \tag{2}$$

$$\mathbf{i} = \mathbf{f}(\mathbf{v}), \qquad \mathbf{v} = \mathbf{D}\mathbf{x} + \mathbf{E}\mathbf{u} + \mathbf{F}\mathbf{i}, \tag{3}$$

where $\mathbf{x}$ is a vector representing the state of the system, $\mathbf{u}$ represents the input, and $\mathbf{i}$ represents the contribution from the nonlinear part to the time derivative of the state. In the following examples, choosing $\mathbf{i}$ to be the nonlinear device currents leads to the most convenient derivation of (2), hence the choice of variable name. The devices are voltage-controlled current sources; thus $\mathbf{v}$ represents these controlling voltages. Matrices $\mathbf{A}$, $\mathbf{B}$, $\mathbf{C}$ represent linear combinations of the state, inputs, and nonlinear part that affect the evolution of the state. The nonlinear contribution (3) is defined implicitly with respect to $\mathbf{i}$ and in general also depends on a linear combination of $\mathbf{x}$ and $\mathbf{u}$.

Discretizing (2) by a numerical integration method, solving for $\mathbf{x}_n$ and substituting into (3) results in an implicit system of equations that can be solved for $\mathbf{i}$. Under conditions presented in [3] amounting to the existence of a unique solution, $\mathbf{i}$ can be expressed as a function of a parameter $\mathbf{p}_n$.

2.2.2. Computational algorithm

If the trapezoidal rule is used to discretize the time derivative in (2), state update comprises the following three-step procedure

1. $\mathbf{p}_n = \mathbf{DH}(\alpha\mathbf{I}+\mathbf{A})\mathbf{x}_{n-1}+(\mathbf{DHB}+\mathbf{E})\mathbf{u}_n+\mathbf{DHB}\mathbf{u}_{n-1}+\mathbf{DHC}\mathbf{i}_{n-1}$
2. $\mathbf{i}_n = \mathbf{g}(\mathbf{p}_n)$
3. $\mathbf{x}_n = \mathbf{H}(\alpha\mathbf{I}+\mathbf{A})\mathbf{x}_{n-1} + \mathbf{HB}(\mathbf{u}_n + \mathbf{u}_{n-1}) + \mathbf{HC}(\mathbf{i}_n + \mathbf{i}_{n-1})$

where subscripts denote the time index, $\mathbf{H} = (\alpha\mathbf{I} - \mathbf{A})^{-1}$, $\alpha = 2/T$ if no prewarping is used, and $\mathbf{i}_n = \mathbf{g}(\mathbf{p}_n)$ is an implicitly defined transformation of $\mathbf{f}(\mathbf{v})$,

$$\mathbf{i}_n = \mathbf{f}(\mathbf{K}\mathbf{i}_n + \mathbf{p}_n), \tag{4}$$

due to the discretization, where $\mathbf{K} = \mathbf{DHC} + \mathbf{F}$. This is a linear transformation of states and inputs to generate an effective input to the original nonlinear function $\mathbf{f}$. Function $\mathbf{g}(\mathbf{p}_n)$ sometimes can be found analytically from (4), but usually needs to be solved numerically by Newton's method or, if possible, fixed point iteration [13]. The state update then takes the past state, present input, and nonlinear contributions to compute the present state.

The output y is generally expressed as a linear combination of the states, inputs, and nonlinear part,

$$\mathbf{y}_n = \mathbf{A}_o\mathbf{x}_n + \mathbf{B}_o\mathbf{u}_n + \mathbf{C}_o\mathbf{i}_n.$$

Once this procedure is defined, only the matrices $\mathbf{A}$, $\mathbf{B}$, $\mathbf{C}$, $\mathbf{D}$, $\mathbf{E}$, $\mathbf{F}$, $\mathbf{A}_o$, $\mathbf{B}_o$, and $\mathbf{C}_o$ and the function $\mathbf{f}(\mathbf{v})$ need to be given to describe the system under consideration.

2.2.3. Computational complexity

The K-method solution involves matrix multiplies, and contemporary CPU architectures were designed with such operations in mind. The K-method approach stands to benefit greatly from data parallelism at the computer architecture level.

If the coefficient matrices and the nonlinear function in the algorithm outlined in Sec. (2.2.2) are precomputed once, the computational complexity for the linear parts of the system is approximately $O\left(N^2 + NM + NP\right)$, where N is the number of states, M is the number of inputs, and P is the number of nonlinear outputs. This quadratic complexity is a disadvantage compared to the WDF, but the K-method is directly applicable to a broader range of circuits.

3. APPLICATION TO VARIOUS GUITAR CIRCUITS

The following examples apply the WDF and SSMN formulations to various circuits found in guitar electronics. We performed all simulations using custom code in MATLAB and utilized Newton's method to solve any nonlinear equations.

3.1. Bright switch/filter

The bright switch (Fig. 3) is commonly found in guitar amplification circuits and sometimes in the electronics of the electric guitar itself as part of a volume knob implemented as a resistive voltage divider. When engaged, it provides a low impedance path for high frequencies to bypass part of the voltage divider.

The WDF tree for the bright switch is shown in Fig. 4 and its signal processing algorithm can be derived by inspection from this tree. The capacitor was chosen to be at the top of the tree because, when it is disconnected, the open circuit at the top of

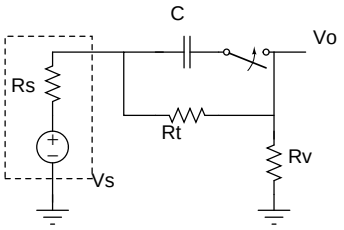

Figure 3: Schematic of the bright switch from guitar electronics.

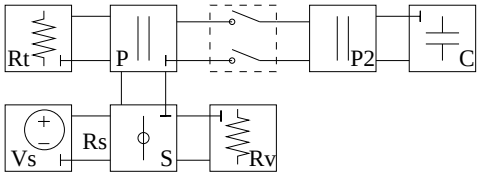

Figure 4: WDF tree to implement the bright switch. Adaptor P2 is root.

the tree produces an instantaneous reflection. Using the reflection-free wave digital capacitor sets its port impedance and requires a parallel two-port adapter P2 to match the impedance of the rest of the tree. The bright switch is suited to implementation as a WDF because of its switched nature. The computational blocks in a WDF correspond directly to the physical circuit elements, which can easily be rearranged to reflect a different structure.

Figure 5 shows the magnitude response of the bright switch simulated using the values $C = 120\text{pF}$, $R_t = (1 - \text{vol})\text{M}\Omega$, $R_v = (\text{vol})\text{M}\Omega$, $R_s = 100\text{k}\Omega$, where $\text{vol} \in [0, 1]$ is the value of the volume potentiometer.

3.2. Two-capacitor diode clipper

The behavior of various numerical methods applied to the single capacitor diode clipper was previously studied extensively [7]. Here we consider the diode clipper including the effects of the DC blocking capacitor. The nonlinearities cause the pole of the high-pass frequency to move depending on the signal level. Because this pole is at low frequencies, this could have a notably audible effect, especially in the presence of transients.

The two-capacitor diode clipper is shown in Fig. 6. The two

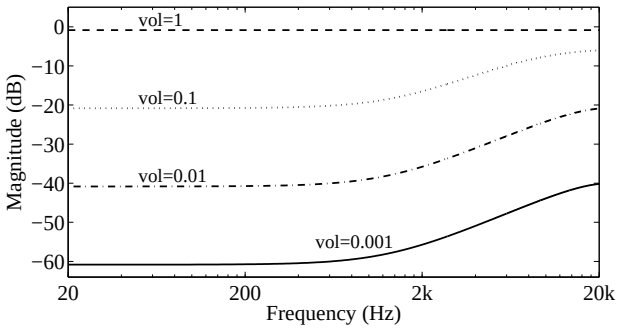

Figure 5: Magnitude response of the volume attenuator with bright switch engaged for values of volume as shown.

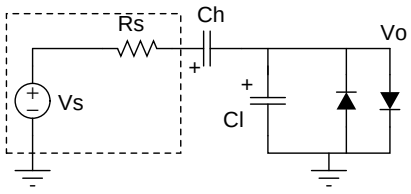

Figure 6: Schematic of the diode clipper with high-pass and low-pass capacitors.

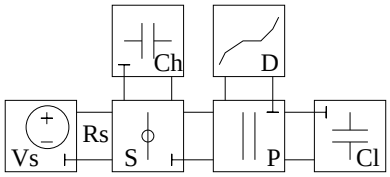

Figure 7: WDF tree of the two-capacitor diode clipper. Diode D is root.

diodes are two physically separate nonlinearities but can be combined into a single equivalent nonlinearity summing their currents by KCL because they are connected in parallel. In the WDF, the two diodes are modeled by the voltage-controlled current source

$$I_d(V) = 2I_s \sinh\left(V/V_t\right), \tag{5}$$

where $I_d(V)$ is the current through the two diodes, I_s and $V_t$are physical parameters of the diodes, and V is the controlling voltage across the diodes.

Device parameters for the following simulations are $R_s = 2.2\text{k}\Omega$, $C_h = 0.47\mu\text{F}$, $C_l = 0.01\mu\text{F}$, $I_s = 2.52 \times 10^{-9}\text{A}$, and $V_t = 45.3\text{mV}$.

3.2.1. WDF implementation

The current state of WDF technology is well suited for modeling circuits connected in series and parallel and with a single one-port nonlinearity. The diode clipper is a prime example of this. The tree corresponding to the computational structure of the WDF for the diode clipper is shown in Fig. 7. The input is the voltage source V_s and the output is the junction voltage of the parallel adaptor.

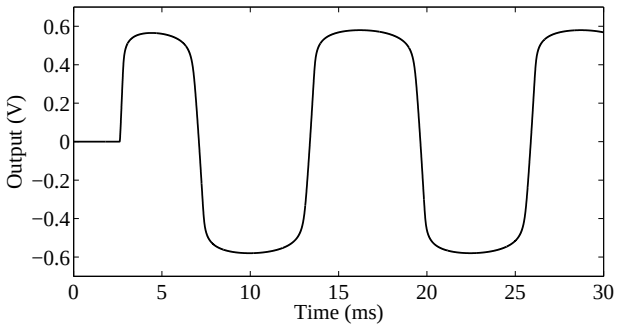

Figure 8: Simulated output of two-capacitor diode clipper for sine input with frequency 80 Hz, amplitude 4.5 V. Identical output is produced by WDF and K-method.

The nonlinear relationship between the incident and reflected waves to this block in the WDF is derived by substituting the wave variable definitions (1) into (5) and solving the resulting implicitly defined nonlinear function for $b = f(a)$ using numerical methods. Specifically, the nonlinear equation to be solved is

$$2I_s \sinh\left(\frac{a+b}{2V_t}\right) - \frac{a-b}{2R_p} = 0.$$

Conditions for which a solution exists are given in [1, 15].

This nonlinear relationship $b = f(a)$ is then placed at the top of the tree representing the rest of the diode clipper to prevent delay-free loops in the signal processing algorithm.

This example demonstrates the power of the WDF formulation to build up algorithms modularly to simulate circuits. The additional high-pass capacitor C_h is added to the single capacitor diode clipper by replacing the original resistive voltage source (inside the dotted box in Fig. 6) with the series combination of the source and the capacitor. Thus, the structure of the WDF derives directly from the connectivity of the modeled circuit.

3.2.2. K-Method implementation

The matrices for the K-method representation of the diode clipper can be found by application of KCL at the two nodes with unknown voltages.

These equations are

$$I_{Ch} = C_h \dot{V}_{Ch} = G_s(V_s - V_x)$$
$$C_l \dot{V}_o = C_h \dot{V}_{Ch} - I_d(V_o).$$

Choosing the state variables to be the voltages across the two capacitors $\mathbf{x} = \begin{bmatrix} V_o & V_{Ch} \end{bmatrix}^T$ with the polarity of the voltages indicated by + on the capacitors in Fig. 6, we solve for $\dot{V}_o$ and $\dot{V}_{Ch}$ using $V_x = V_o + V_{Ch}$ to define the intermediate node voltage in terms of the state variables, and set $u = V_s$ to be the input. We let the nonlinear part $i = I_d(V_o)$, which makes $v = V_o$ the input to the nonlinearity. The state variable V_o is also the output.

$$\dot{V}_o = \frac{G_s}{C_l}(V_s - V_o - V_{Ch}) - \frac{1}{C_l} I_d(V_o)$$
$$\dot{V}_{Ch} = \frac{G_s}{C_h}(V_s - V_o - V_{Ch})$$

The resulting K-method matrices are

$$\mathbf{A} = \begin{bmatrix} -G_s/C_l & -G_s/C_l \\ -G_s/C_h & -G_s/C_h \end{bmatrix}, \qquad \mathbf{D} = \begin{bmatrix} 1 & 0 \end{bmatrix},$$
$$\mathbf{B} = \begin{bmatrix} G_s/C_l \\ G_s/C_h \end{bmatrix}, \qquad \mathbf{E} = \begin{bmatrix} 0 \end{bmatrix},$$
$$\mathbf{C} = \begin{bmatrix} -1/C_l \\ 0 \end{bmatrix}, \qquad \mathbf{F} = \begin{bmatrix} 0 \end{bmatrix}.$$

3.2.3. Simulation results

The output of the diode clipper simulated using an input signal of 80 Hz, 4.5 V amplitude, is plotted in Fig. 8. The sampling rate was $8\times$ oversampled the audio sampling rate of 48000 Hz to reduce signal aliasing in the output. Identical output was produced by the nonlinear WDF and the K-method. Notice the first cycle of the output has a different period than the steady-state response, indicating that the high-pass capacitor does indeed affect the response of the circuit to transients and should be included in models.

3.2.4. Comparative discussion

The signal flow diagram to update the state for both methods involve linear operations followed by a static nonlinearity and more linear operations. The nonlinearity is also present in the discrete-time feedback loop, which alters the order of the nonlinearity.

Considering the nonlinearity as a separate operation of comparable cost, the WDF requires only 4 multiplies and 8 adds to implement the diode clipper. In contrast, the K-method using a straightforward implementation of matrix-vector multiplication requires 13 multiplies and 12 adds. However, it is not straightforward to derive WDFs for the examples that follow.

3.3. Common-emitter transistor amplifier with feedback

Figure 9 shows the common-emitter amplification stage from the Boss DS-1 [12], which employs a bipolar junction transistor (BJT) in the shunt-shunt feedback configuration, giving rise to a transimpedance amplifier. The feedback resistor exists mainly to bias the base of the BJT at a desired operating point. The circuit also features mild emitter degeneration as is common with these amplifiers, which reduces the gain and improves the small-signal linearity of the stage. Because of the high gain from node b to node c, this stage is highly sensitive to the DC bias voltage of node b, which is determined by the design of the circuit. Using incorrect resistor values affects the output swing, which in turn influences the shape and symmetry of the clipped output.

The design values for this circuit are $R_i = 100\text{k}\Omega$, $R_c = 10\text{k}\Omega$, $R_l = 100\text{k}\Omega$, $R_f = 470\text{k}\Omega$, $R_e = 22\Omega$, $C_i = 0.047\mu\text{F}$, $C_f = 250p\text{F}$, and $C_o = 0.47\mu\text{F}$.

3.3.1. Bipolar Junction Transistor (BJT) device model

Figure 10 depicts generic model for the bipolar junction transistor comprising voltage-controlled current sources. The BJT has three terminals, the collector, base, and emitter, whose currents are controlled by voltages across two pairs of the terminals, $V_{be} = V_b - V_e$, $V_{bc} = V_b - V_c$. By conservation of current, only two of the terminal current definitions are needed to completely describe the current-voltage (I-V) characteristics. We use $I_b(V_{be}, V_{bc})$ and $I_c(V_{be}, V_{bc})$ here. Semiconductor devices such as the BJT also have nonlinear resistances and capacitors, which require more detailed models; however, for simplicity, we assume that we can neglect these effects for the signal levels of this circuit in the audio frequency band.

A complete, yet simple, physically derived model for computer simulation, the Ebers-Moll model [18] defines the following current-voltage (I-V) characteristics:

$$I_e = \frac{I_S}{\alpha_F}\left[\exp\left(V_{be}/V_T\right) - 1\right] - I_S\left[\exp\left(V_{bc}/V_T\right) - 1\right] \quad (6)$$
$$I_c = I_S\left[\exp\left(V_{be}/V_T\right) - 1\right] - \frac{I_S}{\alpha_R}\left[\exp\left(V_{bc}/V_T\right) - 1\right] \quad (7)$$
$$I_b = \frac{I_S}{\beta_F}\left[\exp\left(V_{be}/V_T\right) - 1\right] + \frac{I_S}{\beta_R}\left[\exp\left(V_{bc}/V_T\right) - 1\right] \quad (8)$$

Device parameters for this simulation are $V_T = 26\text{mV}$, $\beta_F = 200$, $\beta_R = 0.1$, $\alpha_R = \beta_R/\left(1 + \beta_R\right)$, $I_s = 6.734 \times 10^{-15}\text{A}$. The reader is referred to textbooks on electronic devices, e.g., [18], for detailed interpretation of these parameters.

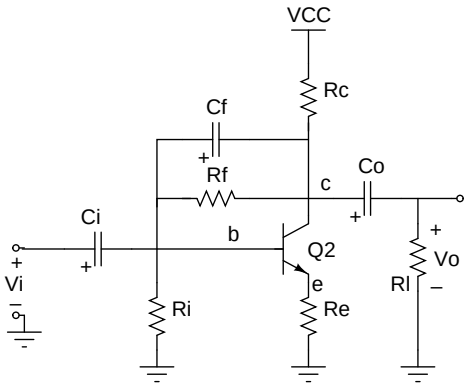

Figure 9: Schematic of the common-emitter amplifier with feedback.

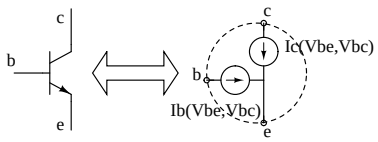

Figure 10: Generic BJT device model.

3.3.2. K-Method formulation

Using the generic description of Fig. 10 for I-V characteristics, we find the K-method matrices for this circuit. Again defining the state to be the voltages across each of the three capacitors, $\mathbf{x} = \begin{bmatrix} V_{Ci} & V_{bc} & V_{Co} \end{bmatrix}^T$ with the polarity of the voltages indicated by + on the capacitors in Fig. 9, we can use KCL to find equations at each of the nodes, and solve for $\dot{\mathbf{x}}$. The inputs are $\mathbf{u} = \begin{bmatrix} V_i & V_{CC} \end{bmatrix}^T$, the input voltage and the supply rail. The nonlinearity is given by

$$\mathbf{i} = \begin{bmatrix} I_b(V_{be}, V_{bc}) & I_c(V_{be}, V_{bc}) \end{bmatrix}^T,$$

the currents at the base and collector terminals of the BJT, and requires an input $\mathbf{v} = \begin{bmatrix} V_{be} & V_{bc} \end{bmatrix}^T$. The output is found from

$$V_o = V_i - V_{Ci} - V_{bc} - V_{Co}.$$

The K-method matrices then give the appropriate linear combinations of these variables using conductance $G_x = 1/R_x$ in place of the corresponding resistance:

$$\mathbf{A} = \begin{bmatrix} -\frac{G_c+G_l+G_i}{C_i} & -\frac{G_c+G_l}{C_i} & -\frac{G_l}{C_i} \\ -\frac{G_c+G_l}{C_f} & -\frac{G_c+G_l+G_f}{C_f} & -\frac{G_l}{C_f} \\ -\frac{G_l}{C_o} & -\frac{G_l}{C_o} & -\frac{G_l}{C_o} \end{bmatrix},$$

$$\mathbf{B} = \begin{bmatrix} \frac{G_c+G_l+G_i}{C_i} & -\frac{G_c}{C_i} \\ \frac{G_c+G_l}{C_f} & -\frac{G_c}{C_f} \\ \frac{G_l}{C_o} & 0 \end{bmatrix}, \quad \mathbf{D} = \begin{bmatrix} -1 & 0 & 0 \\ 0 & 1 & 0 \end{bmatrix},$$

$$\mathbf{E} = \begin{bmatrix} 1 & 0 \\ 0 & 0 \end{bmatrix},$$

$$\mathbf{C} = \begin{bmatrix} 1/C_i & 1/C_i \\ 0 & 1/C_f \\ 0 & 0 \end{bmatrix}, \quad \mathbf{F} = \begin{bmatrix} -R_e & -R_e \\ 0 & 0 \end{bmatrix}.$$

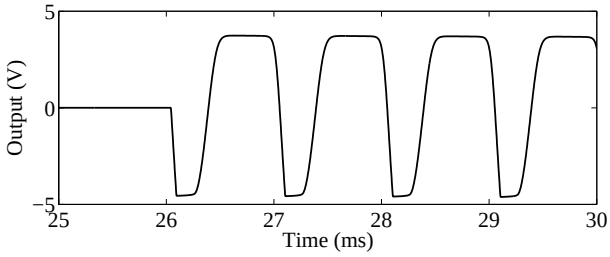

Figure 11: Output of the common-emitter amplifier for sine input of 0.2 V, 1 kHz.

The formulation given admits a generic device model. While the Ebers-Moll model for a BJT is used here specifically, it is a simple model that does not account for the many nonidealities of real devices. In practice, the distortion performance of the circuit is highly sensitive to the accuracy of the device models, which usually represent some simplification of reality. This formulation allows for the use of tabulated device models obtained experimentally for greatest accuracy.

3.3.3. Simulation results

The BJT amplifier was simulated at a sampling rate of $8\times$ the audio rate 48000 Hz. The results are shown in Fig. 11. Note the asymmetry of the duty cycle of the output given a sine wave input. This is due to the asymmetry in the nonlinearity: one polarity clips at a lower level than the other. This injects an offset at DC, which is being filtered out by the DC blocking capacitor at the output, causing the the bias of the output waveform to shift downward after the initial transient at 26 ms (not shown). A slowly shifting bias would affect the distortion of subsequent nonlinear stages.

3.4. Common-cathode triode amplifier with supply bypass

In guitar circuits, the ubiquitous common-cathode triode amplifier stage (Fig. 12) provides preamplification gain. Several of these stages can be cascaded for a high-gain amplifier. This circuit is essentially the same configuration as a BJT common-emitter amplifier. The grid resistor R_g and parasitic Miller capacitance C_f are shown explicitly in this simulation circuit. The cathode resistor R_k determines the operating bias point for the circuit. Often a bypass capacitor C_k is placed across the cathode resistor to counteract the effects of gain degeneration caused by the resistor, and gives a bandpass gain.

For this simulation, the circuit design used is $R_g = 70\text{k}\Omega$, $R_k = 1500\Omega$, $R_p = 100\text{k}\Omega$, $R_i = 1\text{M}\Omega$, $C_i = 0.047\mu\text{F}$, $C_f = 2.5p\text{F}$, $C_k = 25\mu\text{F}$.

3.4.1. Triode device model

The triode differs slightly from the BJT in the device model. While the BJT is controlled by the voltages across the base-emitter, and base-collector ports, owing to different operating principles, the triode is controlled by the voltages across the gate-cathode and cathode-anode ports. The triode device model is shown in Fig. 13.

The classic Child-Langmuir triode equation for the plate cur-

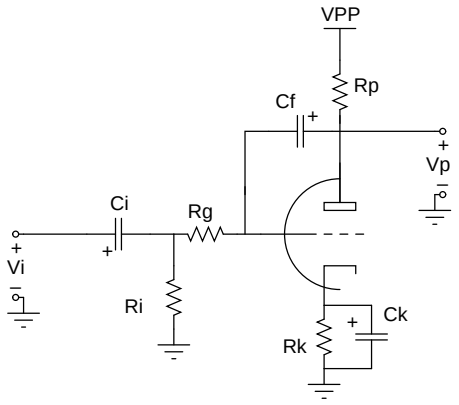

Figure 12: Schematic of the common-cathode triode amplifier.

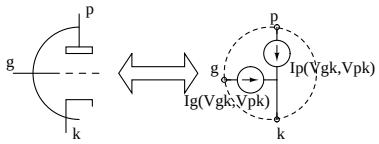

Figure 13: Generic triode device model.

rent [19] is used here as a proof of concept:

$$I_p = K\left(E_d\left(\frac{1+\text{sign}(E_d)}{2}\right)\right)^{3/2}, \quad \text{where}$$

$$E_d = \mu V_{gk} + V_{pk},$$

and grid current $I_g = 0$. For the 12AX7 triode in this simulation, $\mu = 83.5$, $K = 1.73 \times 10^{-6}\text{A/V}^{3/2}$ [20].

The Child-Langmuir model allows the plate-cathode voltage to become negative while plate-cathode current is positive when the grid voltage is sufficiently high. This unphysical behavior demonstrates the inaccuracy of the model in a common region of operation for guitar distortion.

The Child-Langmuir equation is admittedly a poor model for simulation; however, the K-method formulation admits a general two-port description of the triode, so any of the multitude of triode models developed for circuit simulation in SPICE can be ported to this method. In particular, this formulation accounts for the effects of grid conduction (not used with this model), which is claimed to be sonically significant [21].

3.4.2. K-method formulation

While a similar circuit was simulated using the wave digital formulation [9], the two-port nonlinear device does not yet readily admit a wave digital representation, and ad-hoc means were necessary to generate a WDF. Alternatively, the K-method allows direct simulation of the common-cathode circuit in Fig. 12.

The state vector is the voltages across each of the capacitors $\mathbf{x} = \begin{bmatrix} V_{Ci} & V_{Cf} & V_{Ck} \end{bmatrix}^T$, with the polarity of the voltages indicated by + on the capacitors in Fig. 12. The inputs are $\mathbf{u} = \begin{bmatrix} V_i & V_{PP} \end{bmatrix}^T$, the input voltage and the supply rail. The nonlinearity is given by

$$\mathbf{i} = \begin{bmatrix} I_g(V_{gk}, V_{pk}) & I_p(V_{gk}, V_{pk}) \end{bmatrix}^T,$$

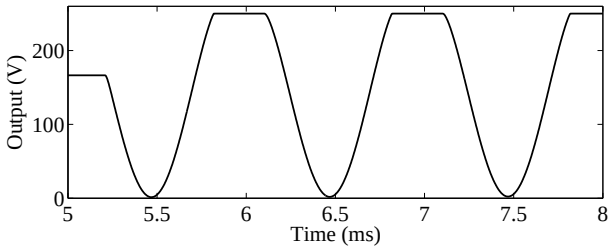

Figure 14: Plate voltage of common-cathode amplifier for sine input of 2.8 V, 1000 Hz.

the currents through the grid and plate terminals, and requires an input $\mathbf{v} = \begin{bmatrix} V_{gk} & V_{pk} \end{bmatrix}^T$, the voltages across the grid-cathode, and plate-cathode ports. The K-method matrices, using conductance $G_x = 1/R_x$ in place of the corresponding resistance, are then

$$\mathbf{A} = \begin{bmatrix} \frac{-\left((G_i+G_g)G_p+G_iG_g\right)}{C_i(G_g+G_p)} & \frac{G_gG_p}{C_i(G_g+G_p)} & 0 \\ \frac{G_gG_p}{C_f(G_g+G_p)} & \frac{-G_gG_p}{C_f(G_g+G_p)} & 0 \\ 0 & 0 & \frac{-G_k}{C_k} \end{bmatrix},$$

$$\mathbf{B} = \begin{bmatrix} \frac{\left((G_i+G_g)G_p+G_iG_g\right)}{C_i(G_g+G_p)} & \frac{-G_gG_p}{C_i(G_g+G_p)} \\ \frac{-G_gG_p}{C_f(G_g+G_p)} & \frac{G_gG_p}{C_f(G_g+G_p)} \\ 0 & 0 \end{bmatrix},$$

$$\mathbf{C} = \begin{bmatrix} \frac{G_g}{C_i(G_g+G_p)} & \frac{G_g}{C_i(G_g+G_p)} \\ \frac{G_p}{C_f(G_g+G_p)} & \frac{-G_g}{C_f(G_g+G_p)} \\ \frac{1}{C_k} & \frac{1}{C_k} \end{bmatrix},$$

$$\mathbf{D} = \begin{bmatrix} \frac{-G_g}{G_p+G_g} & \frac{-G_p}{G_p+G_g} & -1 \\ \frac{-G_g}{G_p+G_g} & \frac{G_g}{G_p+G_g} & -1 \end{bmatrix},$$

$$\mathbf{E} = \begin{bmatrix} \frac{G_g}{G_p+G_g} & \frac{G_p}{G_p+G_g} \\ \frac{G_g}{G_p+G_g} & \frac{G_p}{G_p+G_g} \end{bmatrix}, \quad \mathbf{F} = \begin{bmatrix} \frac{-1}{G_p+G_g} & \frac{-1}{G_p+G_g} \\ \frac{-1}{G_p+G_g} & \frac{-1}{G_p+G_g} \end{bmatrix}.$$

The output is taken to be the plate voltage and can be found by $V_{pk} + V_k$ during simulation. This output contains a bias voltage and needs to be high-pass filtered for use in an audio plugin.

3.4.3. Simulation results

The tube preamp was simulated using the Child-Langmuir triode model at a sampling rate of $8\times$ the audio rate 48000 Hz. The plate voltage for an input of 2.8 V, 1000 Hz, is plotted in Fig. 14. Notice that this device model has an unrealistically sharp cutoff, leading to the truncated tops of the waveforms in the figure.

4. CONCLUSIONS

The nonlinear methods developed for computational musical acoustics are readily applied to musical circuits simulation. For accurate simulation, these methods require electronic device equations that accurately model the nonlinearities. Device models for bipolar junction transistors were designed with circuit simulation in mind. This is not the case with currently available vacuum-tube

models, which tend to result in unreliable simulations due to discontinuities in the model or poorly behaved regions in the curve fits. Vacuum-tube device models need to be improved before nonlinear computer simulation of vacuum-tube circuits can become realistic. Once accurate, numerically robust device models are available, they can be readily used with these two methods for solving nonlinear ordinary differential equations.

Wave digital filters offer computational efficiency, robustness to coefficient quantization, and facilitate interfacing with wave variables, making them a worthwhile subject of study. Representation of multiport nonlinearities is still under investigation.

For the K-method, states should correspond to the natural state elements of the circuit, namely capacitors and inductors. Choosing the appropriate state variables facilitates derivation of the nonlinear state-space equations and aids interpretation of the resulting system.

For solving nonlinear systems, both methods are conceptually similar in the overall order of operations. Both first compute a linear combination of state and inputs – this is used as a parameter to a nonlinear function. Then to update the states they compute linear combinations of these variables with the outputs of the nonlinearity.

Circuits are made of canonical building blocks, which can be identified. Circuits can be decomposed into stages by inspection of the schematic for these building blocks. Loading between stages (a form of feedback), and local and global feedback can be accounted for by using nonlinear filter composition. The next step is to build simulations of the full signal path of a guitar distortion circuit and evaluate its real-time performance and reliability.

Further work can be done comparing the performance of these simulation approaches against established circuit simulation algorithms.

5. ACKNOWLEDGMENTS

Thanks to Profs. Matti Karjalainen, Davide Rocchesso, and Augusto Sarti for fruitful discussions regarding the comparative merits of these methods. Thanks also to the AkuLab at TKK for kindly hosting the first author's visit during the formative period for these ideas, supported by a National Science Foundation Graduate Fellowship.

6. REFERENCES

[1] A. Sarti and G. De Poli, "Toward nonlinear wave digital filters," *IEEE Trans. Signal Process.*, vol. 47, pp. 1654–1668, June 1999.

[2] G. De Sanctis, A. Sarti, and S. Tubaro, "Automatic synthesis strategies for object-based dynamical physical models in musical acoustics," in *Proc. of the Int. Conf. on Digital Audio Effects (DAFx-03)*, London, UK, Sept. 2003.

[3] G. Borin, G. De Poli, and D. Rocchesso, "Elimination of delay-free loops in discrete-time models of nonlinear acoustic systems," *IEEE Trans. Speech and Audio Proc.*, vol. 8, no. 5, pp. 597–605, Sept. 2000.

[4] F. Fontana, F. Avanzini, and D. Rocchesso, "Computation of nonlinear filter networks containing delay-free paths," in *Proc. Conf. on Digital Audio Effects (DAFx-04)*, Naples, Italy, Oct. 2004, pp. 113–118.

[5] A. Huovilainen, "Enhanced digital models for analog modulation effects," in *Proc. of the Int. Conf. on Digital Audio Effects (DAFx-05)*, Madrid, Spain, Sept. 20-22 2005, pp. 155–160.

[6] F. Avanzini and D. Rocchesso, "Efficiency, accuracy, and stability issues in discrete time simulations of single reed instruments," *J. of the Acoustical Society of America*, vol. 111, no. 5, pp. 2293–2301, May 2002.

[7] D. T. Yeh, J. S. Abel, A. Vladimirescu, and J. O. Smith, "Numerical Methods for Simulation of Guitar Distortion Circuits," *Computer Music Journal*, vol. 32, no. 2, pp. 23–42, 2008.

[8] A. Huovilainen, "Nonlinear digital implementation of the Moog ladder filter," in *Proc. of the Int. Conf. on Digital Audio Effects (DAFx-04)*, Naples, Italy, Oct. 5–8, 2004, pp. 61–64.

[9] M. Karjalainen and J. Pakarinen, "Wave digital simulation of a vacuum-tube amplifier," in *IEEE ICASSP 2006 Proc.*, Toulouse, France, 2006, vol. 5, pp. 153–156.

[10] J. Pakarinen, *Modeling of Nonlinear and Time-Varying Phenomena in the Guitar*, Ph.D. thesis, Helsinki University of Technology, 2008.

[11] R. Rabenstein, S. Petrausch, A. Sarti, G. De Sanctis, C. Erkut, and M. Karjalainen, "Block-Based Physical Modeling for Digital Sound Synthesis," *IEEE Signal Process. Mag.*, vol. 24, no. 2, pp. 42–54, Mar. 2007.

[12] D. T. Yeh, J. Abel, and J. O. Smith, "Simplified, physically-informed models of distortion and overdrive guitar effects pedals," in *Proc. of the Int. Conf. on Digital Audio Effects (DAFx-07)*, Bordeaux, France, Sept. 10–14, 2007.

[13] F. Avanzini, F. Fontana, and D. Rocchesso, "Efficient computation of nonlinear filter networks with delay-free loops and applications to physically-based sound models," in *Proc. of The Fourth Int. Wkshp. on Multidim. Sys., (NDS 2005)*, Wuppertal, Germany, July 2005, pp. 110–115.

[14] A. Fettweis, "Wave digital filters: Theory and practice," *Proc. IEEE*, vol. 74, no. 2, pp. 270 – 327, Feb. 1986.

[15] K. Meerkötter and R. Scholz, "Digital simulation of nonlinear circuits by wave digital filter principles," in *Proc. IEEE Int. Symp. on Circuits and Systems*, May 1989, vol. 1, pp. 720–723.

[16] S. Petrausch and R. Rabenstein, "Wave digital filters with multiple nonlinearities," in *XII European Sig. Proc. Conf. (EUSIPCO)*, Vienna, Austria, Sept. 2004, vol. 1, pp. 77–80.

[17] T. Felderhoff, "A new wave description for nonlinear elements," in *IEEE Int. Symp. on Circuits and Systems (ISCAS '96)*, Atlanta, USA, May 1996, vol. 3, pp. 221–224.

[18] R. S. Muller, T. L. Kamins, and M. Chan, *Device Electronics for Integrated Circuits*, Wiley, Hoboken, NJ, 3 edition, 2002.

[19] K. Spangenberg, *Vacuum Tubes*, McGraw-Hill, New York, 1st edition, 1948.

[20] W. M. Leach, "SPICE Models for Vacuum-Tube Amplifiers," *J. Audio Eng. Soc.*, vol. 43, no. 3, pp. 117–126, May 1995.

[21] J.-C. Maillet, "A generalized algebraic technique for modeling triodes," *Glass Audio*, vol. 10, no. 2, pp. 2–9, 1998.